



# Kent Academic Repository

Dawes, Anita, Pascual, Natalia, Hoffmann, Søren V., Jones, Nykola C. and Mason, Nigel J. (2017) *Vacuum ultraviolet photoabsorption spectroscopy of crystalline and amorphous benzene*. *Physical Chemistry Chemical Physics*, 19 (40). pp. 27544-27555. ISSN 1463-9076.

## Downloaded from

<https://kar.kent.ac.uk/74653/> The University of Kent's Academic Repository KAR

## The version of record is available from

<https://doi.org/10.1039/c7cp05319c>

## This document version

Author's Accepted Manuscript

## DOI for this version

## Licence for this version

UNSPECIFIED

## Additional information

## Versions of research works

### Versions of Record

If this version is the version of record, it is the same as the published version available on the publisher's web site. Cite as the published version.

### Author Accepted Manuscripts

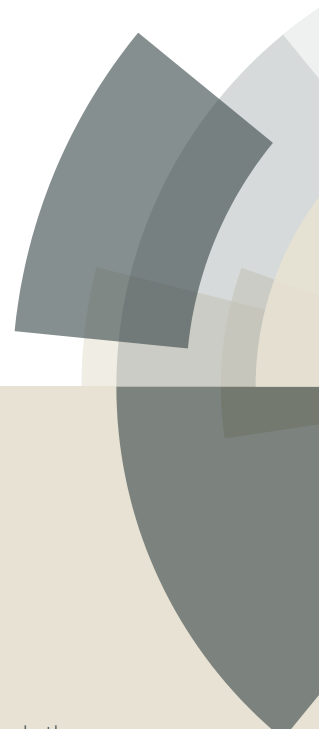
If this document is identified as the Author Accepted Manuscript it is the version after peer review but before type setting, copy editing or publisher branding. Cite as Surname, Initial. (Year) 'Title of article'. To be published in *Title of Journal*, Volume and issue numbers [peer-reviewed accepted version]. Available at: DOI or URL (Accessed: date).

## Enquiries

If you have questions about this document contact [ResearchSupport@kent.ac.uk](mailto:ResearchSupport@kent.ac.uk). Please include the URL of the record in KAR. If you believe that your, or a third party's rights have been compromised through this document please see our [Take Down policy](https://www.kent.ac.uk/guides/kar-the-kent-academic-repository#policies) (available from <https://www.kent.ac.uk/guides/kar-the-kent-academic-repository#policies>).

# PCCP

Accepted Manuscript



This article can be cited before page numbers have been issued, to do this please use: A. Dawes, N. Pascual, S. V. Hoffmann, N. C. Jones and N. J. Mason, *Phys. Chem. Chem. Phys.*, 2017, DOI: 10.1039/C7CP05319C.



This is an Accepted Manuscript, which has been through the Royal Society of Chemistry peer review process and has been accepted for publication.

Accepted Manuscripts are published online shortly after acceptance, before technical editing, formatting and proof reading. Using this free service, authors can make their results available to the community, in citable form, before we publish the edited article. We will replace this Accepted Manuscript with the edited and formatted Advance Article as soon as it is available.

You can find more information about Accepted Manuscripts in the [author guidelines](#).

Please note that technical editing may introduce minor changes to the text and/or graphics, which may alter content. The journal's standard [Terms & Conditions](#) and the ethical guidelines, outlined in our [author and reviewer resource centre](#), still apply. In no event shall the Royal Society of Chemistry be held responsible for any errors or omissions in this Accepted Manuscript or any consequences arising from the use of any information it contains.

Cite this: DOI: 10.1039/xxxxxxxxxx

## Vacuum ultraviolet photoabsorption spectroscopy of crystalline and amorphous benzene

Anita Dawes,<sup>\*a</sup> Natalia Pascual,<sup>a,b</sup> Søren V. Hoffmann<sup>c</sup>, Nykola C. Jones<sup>c</sup> and Nigel J. Mason<sup>a</sup>

Received Date

Accepted Date

DOI: 10.1039/xxxxxxxxxx

www.rsc.org/journalname

We present the first high resolution vacuum ultraviolet photoabsorption study of amorphous benzene with comparisons to annealed crystalline benzene and the gas phase. Vapour deposited benzene layers were grown at 25 K and annealed to 90 K under conditions pertinent to interstellar icy dust grains and icy planetary bodies in our Solar System. Three singlet-singlet electronic transitions in solid benzene correspond to the  ${}^1B_{2u}$ ,  ${}^1B_{1u}$  and  ${}^1E_{1u}$  states, redshifted by 0.05, 0.25 and 0.51 eV respectively with respect to the gas phase. The symmetry forbidden  ${}^1B_{2u} \leftarrow {}^1A_{1g}$  and  ${}^1B_{1u} \leftarrow {}^1A_{1g}$  transitions exhibit vibronic structure due to vibronic coupling and intensity borrowing from the allowed  ${}^1E_{1u} \leftarrow {}^1A_{1g}$  transition. Additionally the  ${}^1B_{2u} \leftarrow {}^1A_{1g}$  structure shows evidence of coupling between intramolecular vibrational and intermolecular lattice modes in crystalline benzene with Davydov crystal field splitting observed. The optically forbidden 0–0 electronic origin is clearly visible as a doublet at 4.69/4.70 eV in the crystalline solid and as a weak broadened feature at 4.67 eV in amorphous benzene. In the case of the  ${}^1B_{1u} \leftarrow {}^1A_{1g}$  transition the forbidden 0–0 electronic origin is only observed in crystalline benzene as an exciton peak at 5.77 eV. Thicker amorphous benzene samples show diffuse bands around 4.3, 5.0 and 5.4 eV that we tentatively assign to spin forbidden singlet-triplet  ${}^3B_{2u} \leftarrow {}^1A_{1g}$ ,  ${}^3E_{1u} \leftarrow {}^1A_{1g}$  and  ${}^3B_{1u} \leftarrow {}^1A_{1g}$  transitions respectively, not previously reported in photoabsorption spectra of amorphous benzene. Furthermore, our results show clear evidence of non-wetting or ‘islanding’ of amorphous benzene, characterised by thickness-dependent Rayleigh scattering tails at wavelengths greater than 220 nm. These results have significant implications for our understanding of the physical and chemical properties and processes in astrochemical ices and highlight the importance of VUV spectroscopy.

### 1 Introduction

Benzene is a prototypical aromatic organic molecule that forms the basis of many organic and biological molecules and has therefore attracted much computational and experimental work in physical chemistry over the past 70 years in order to unravel its electronic structure (in-depth reviews with historical developments are found in references<sup>1,2</sup>). Most of the experimental work reported on benzene in the literature involves either the gas phase or the crystalline phase with little systematic analysis of the amorphous phase. Our present work focuses on the electronic structure of condensed molecules pertinent to icy surfaces in the

interstellar medium (ISM) and Solar System bodies encompassed by the interdisciplinary field of astrochemistry. Much of the laboratory work in the field of astrochemistry focuses on infrared spectroscopy and temperature programmed desorption studies to learn about the physical and chemical properties of condensed molecules on cold surfaces<sup>3</sup>. However our work has shown that vacuum ultraviolet (VUV) spectroscopy can also be a powerful tool in understanding the properties of condensed films<sup>4</sup>. The aim of this work is to exploit VUV spectroscopy, to carry out a systematic study to understand the chemical and physical properties and structure of amorphous and crystalline benzene films and make it applicable and accessible to the astrochemistry community.

Benzene constitutes the simplest aromatic unit and is a building block of polycyclic aromatic hydrocarbons (PAHs). PAHs are ubiquitous in the interstellar medium (ISM)<sup>5,6</sup>, being the most abundant molecules after molecular hydrogen and carbon monoxide and are estimated to account for up to 30% of the interstellar

<sup>a</sup> School of Physical Sciences, The Open University, Walton Hall, Milton Keynes, MK7 6AA, UK. Fax: +44 (0)1908 6 54192; Tel: +44 (0)1908 6 54241; E-mail: Anita.Dawes@open.ac.uk

<sup>b</sup> Department of Chemistry and Physics, La Trobe Institute for Molecular Science, La Trobe University, Melbourne 3086, Australia

<sup>c</sup> ISA, Centre for Storage Ring Facilities, Department of Physics and Astronomy, Aarhus University, Ny Munkegade 120, DK-8000 Aarhus C, Denmark.

carbon. They have been observed in great abundance in the gas phase in both galactic and extragalactic ISM via their characteristic infrared emission bands between 3.3 and 18  $\mu\text{m}$  in photon dominated regions. In these regions stable gas phase neutral and ionised PAHs are continuously stimulated by UV photons resulting in emission via infrared (IR) fluorescence. Conversely, little is known about the role of PAHs in solid-state chemistry. Though no individual PAH has yet been identified in the ISM, gas phase benzene has been detected in the torus of the protoplanetary nebula CRL 618<sup>7</sup> and in the Large Magellanic Cloud object SMP LMC 11<sup>8</sup>. Benzene and small condensed phase PAHs are thought to be prevalent in the cold, dense molecular clouds where they are either incorporated into ice mantles or act as nucleation sites for the condensation of other species<sup>9</sup>. Weak IR absorption features attributed to PAHs have been observed in spectra of embedded protostars<sup>10</sup>, and PAHs identified in meteoritic and cometary samples show deuterium enrichment that points to their possible dense molecular cloud origins<sup>11</sup>. PAHs are observed in protoplanetary discs around newly forming stars<sup>12,13</sup> and may either be formed in shocks or are released from icy grains<sup>14</sup>. PAHs are also prevalent in our Solar system, on icy bodies in the Outer Solar System<sup>15</sup> and in comets<sup>16</sup>. They have also been found in carbonaceous meteorites<sup>17</sup>, interplanetary dust particles<sup>18</sup> and in the atmospheres of Titan and Jupiter<sup>19</sup>.

PAH-ice photochemistry has therefore become the topic of numerous laboratory studies demonstrating that PAHs are efficiently ionised in water ice under UV irradiation<sup>20</sup>, with the ionisation energy lowered by up to 2 eV compared to the gas phase<sup>21</sup> and found to be most efficient at lower temperatures (<50K)<sup>22</sup> with PAH cations stable within the ice up to 120K<sup>23</sup>. The PAH carbon skeleton appears to be stable under exposure to ion<sup>24</sup> and UV irradiation<sup>25</sup> although side group addition reactions or dehydrogenation can occur. There is also compelling evidence that PAHs may facilitate desorption of ices<sup>26</sup>. This experiment demonstrated that vibronic excitation of benzene (at 250 nm) resulted in the indirect desorption of undissociated 'hot' water molecules with a translational temperature of 450 K.

In order to fully understand such photochemical and photodesorption processes involving large aromatic molecules such as benzene and PAHs in the solid phase, it is essential to ascertain how UV photons interact with such species. Since ices containing PAHs in interstellar environments are subjected to a broad spectrum of UV radiation, in order to fully understand photochemical processes in such environments, realistic mimics of stellar/solar radiation are necessary to study them in detail and UV spectra over a wide spectral range are required. Our previous laboratory studies have shown that the UV spectra, arising due to the excitation of electronic molecular transitions, of ices prepared under astrophysical conditions show dramatic changes including shifts in peak positions, changes in width and intensity (i.e. photoabsorption cross sections) and the appearance of new bands due to transitions otherwise forbidden in the gas phase spectra<sup>4,27,28</sup>. So the electronic transitions of the molecules within the ice matrix are influenced by factors that affect the ice structure and morphology that is the ice deposition rate and temperature and thermal history.

The goal of this work is to measure the vacuum ultraviolet photoabsorption spectrum of solid benzene in the amorphous and crystalline phases in order to determine photoabsorption cross sections that can be used by the astrochemistry community. This work forms part of a systematic experimental programme to measure the photoabsorption cross sections of PAHs and their derivatives under conditions pertinent to that of icy grain mantles in dense molecular clouds and star forming regions as well as the surfaces of icy satellites in the Outer Solar System. In this paper we report the results of vacuum ultraviolet (VUV) photoabsorption spectroscopy of benzene at 25 K and annealed to higher temperatures.

## 2 Experimental Methods

The experiments were carried out using a portable astrochemistry chamber attached to the AU-UV beamline<sup>29</sup> at the new ASTRID2 Synchrotron Facility in Aarhus, Denmark. A similar set up for investigation of condensed phase molecules has been used previously as described in<sup>28</sup> and only a brief summary any modifications are described here. The experiments were carried out at a base pressure of  $10^{-9}$  mbar. The substrate was held in thermal contact with a cold finger attached to a closed cycle helium cryostat (Sumitomo) with a base temperature of 25 K. Benzene (anhydrous; Sigma-Aldrich, 99.8% purity) was vapour deposited at normal incidence via a 3 mm nozzle 2 cm from the cooled substrate by turning it to face a gas inlet port attached to a gas line where a benzene liquid sample was degassed via three freeze-pump-thaw cycles prior to use.

The vapour flow was regulated with a precision needle valve and deposition rates were  $0.12 \text{ nm s}^{-1}$  for all the samples. The solid benzene film thickness was determined by monitoring the cyclic variation in intensity of a HeNe laser beam reflected off the surface during ice film growth with an angle of incidence of  $20^\circ$ . Interference of the reflected laser beam from the sample vacuum and the substrate-sample interface generates a sinusoidal output as a function of sample thickness. The refractive index of the film,  $n_1$ , is estimated from the ratio of the maxima and the minima of the fitted laser interference pattern<sup>30</sup>. The values of  $n_1$  for the ice films used in this study ranged between 1.38 and 1.47 ( $\pm 0.06$ ) which is close to the experimental value of 1.4925 for liquid benzene (300 K) at 632.8 nm reported by Moutzouris *et al.*<sup>31</sup>. This is used to calculate the angle of the refracted light within the film,  $\theta_1$ . The fit also provides the time in seconds between the maxima,  $w_t$  (s) corresponding to constructive interference. The film thickness  $l$  is then calculated using the following equation:

$$l = \frac{\lambda_0}{2n_1 \cos \theta_1} \times \frac{t}{w_t} \quad (1)$$

where  $\lambda_0$  is the wavelength of the HeNe beam (632.8 nm) in vacuum and  $t$  (s) is the total deposition time. Thicknesses below 40 nm were used for thickness dependent studies described in section 3.3. A 38 nm thick sample was used for all the spectra in the range of 5.5–10.7 eV (225–115 nm) to avoid band saturation and a 301 nm thick sample was used for the spectra in the range of 3.6–5.5 eV (340–225 nm) to resolve the weak features in this region.

Though some background deposition of water is expected at a base chamber pressure of  $10^{-9}$  mbar (a limitation of the portable experimental system) we believe water contamination to be negligible in the spectra of thinner samples due to short deposition times at a background deposition pressure of  $10^{-7}$  mbar. Any water contamination from background deposition during the longer high resolution scans in the thicker samples was not found to affect the benzene spectral features which all lie at wavelengths above the low-energy onset of the water band ( $<165$  nm). Comparison of results (band positions and widths) between the thicker and thinner samples showed no associated shifts that are observed in the spectra of benzene-water mixtures (to appear in a future publication), confirming negligible effects due to any water contamination for the set of data presented here.

The AU-UV beamline, equipped with a grating monochromator, provides a tunable source of polarised VUV light at high resolution. The minimum wavelength at which the cross sections can be measured is determined by the entrance/exit window and substrate materials. For the spectra presented in this paper, a lithium fluoride (LiF) entrance window and a magnesium fluoride ( $\text{MgF}_2$ ) substrate and exit window were used. Thus the minimum wavelengths for which reliable data could be acquired was 10.78 eV (115 nm). The maximum wavelength cutoff was 3.65 eV (340 nm), limited by the grating. All spectra were acquired in 0.1 nm steps and 0.05 nm intervals were used to resolve fine features in the spectrum of benzene between 5.5 and 4.5 eV (225 and 275 nm). Background spectra were collected through the blank clean, cold substrate prior to sample deposition giving the incident intensity  $I_0(\lambda)$ . The transmitted spectra were then measured after sample deposition giving the transmitted intensity,  $I_t(\lambda)$ . The absorbance (natural log scale) was then calculated using the following formula.

$$A = \ln \left( \frac{I_0(\lambda)}{I_t(\lambda)} \right) \quad (2)$$

Both the incident and transmitted signals are corrected for the beam current in the synchrotron ring with the intensity being directly proportional to the electron current. Cross sections  $\sigma(\lambda)$  were calculated using the Beer-Lambert Law:

$$I_t(\lambda) = I_0(\lambda)e^{-\sigma(\lambda)nl} \quad (3)$$

where  $n$  ( $\text{cm}^{-3}$ ) is the number density and  $l$  (cm) is the path-length given by the film thickness determined from Equation 1 converted to cm. We used a density of  $0.94 \text{ g cm}^{-3}$  for solid benzene from Colson *et. al.*<sup>32</sup>.

Samples were annealed gradually at a rate of  $1 \text{ K min}^{-1}$  by heating the sample using a Kapton heater and regulated with a temperature controller (Oxford Instruments). The samples were held at the required temperature for 2 minutes and then the heating was stopped returning the samples to base temperature (25 K) prior to measuring the spectra. This ensures that no further energy is deposited to the samples during data acquisition and any temperature dependence of the substrate, that might alter the spectra, is avoided. The gas phase spectrum used for comparison with the spectra of solid phase benzene was measured

with the same photon resolution at the same beamline using a photoabsorption gas cell.

## 3 Results and Discussion

### 3.1 The electronic structure of solid and gas phase benzene

The ground state of the benzene molecule is  $^1A_{1g}$  with the electronic configuration:  $(2a_{1g})^2 (2e_{1u})^2 (2e_{2g})^4 (3a_{1g})^2 (2b_{1u})^2 (1b_{2u})^2 (3e_{1u})^4 (1a_{2u})^2 (3e_{2g})^4 (1e_{1g})^4$ . The overlap of six carbon  $2p_z$  orbitals, each containing one valence electron, gives rise to  $\pi$  orbitals with the configuration  $(a_{2u})^2 (e_{1g})^4 (e_{2u})^0 (b_{2g})^0$ . A single electron  $\pi^* \leftarrow \pi$  transition from the highest occupied molecular orbital (HOMO) ( $e_{1g}$ ) to the lowest unoccupied molecular orbital (LUMO) ( $e_{2u}$ ) leads to three excited singlet states  $^1B_{2u}$ ,  $^1B_{1u}$  and  $^1E_{1u}$ . These transitions are observed in the vacuum ultraviolet photoabsorption spectrum of benzene between 10.33 and 3.65 eV (120 and 340 nm). The weak  $^1B_{2u}$  and  $^1B_{1u}$  states are dipole symmetry forbidden, however they are observed due to Herzberg-Teller vibronic coupling and intensity borrowing from the allowed  $^1E_{1u}$  state via a vibrational mode with an  $e_{2g}$  symmetry, giving rise to vibronic structure in the  $^1B_{2u} \leftarrow ^1A_{1g}$  and  $^1B_{1u} \leftarrow ^1A_{1g}$  transitions upon UV excitation.

Figure 1 shows the spectrum of solid amorphous benzene deposited at 25 K, the same solid annealed to 90 K (and returned to 25 K) and both spectra compared with the gas phase benzene spectrum. The solid phase spectra show the same three electronic transitions as in the gas phase but there are clearly significant differences in the spectra between the solid and the gas phase arising due to intermolecular interaction between benzene molecules in the solid phase. In the vapour deposited solid benzene at 25 K, all the electronic and vibronic bands are broadened and there is a significant red-shift in the band positions with the maximum shift observed in the  $^1E_{1u}$  band from around 6.97 eV (178 nm) in the gas phase to 6.46 eV (192 nm) in the solid phase corresponding to a shift of 0.51 eV (14 nm). There is considerable broadening and decrease in intensity of this band, with an approximate decrease to 50% in the band area in the solid phase compared to the gas phase. The  $^1B_{1u} \leftarrow ^1A_{1g}$  band shows a smaller shift from around 6.20 to 5.90 eV (200 to 210 nm) corresponding to a shift of 0.30 eV (10 nm), but with a similar intensity and band area compared to the gas phase. Finally the smallest redshift is observed in the vibronic structure associated with the  $^1B_{2u} \leftarrow ^1A_{1g}$  transition around 4.86 eV (255 nm), with an average shift of 0.05 eV (2.6 nm) in the vibronic bands. There are also further shifts and differences in the profiles between the spectra of solid benzene at 25 K and at 90 K, which will be discussed in more detail in section 3.2. The vibronic structure corresponding to the  $^1B_{2u} \leftarrow ^1A_{1g}$  and  $^1B_{1u} \leftarrow ^1A_{1g}$  transitions will be discussed in more detail in sections 3.2.1 and 3.2.2. Interestingly there are also two weak, broad bands visible in the solid phase spectrum around 5.5 eV (290 nm) and 4.3 eV (288 nm) that are not present in the gas phase spectrum. These will be discussed in more detail in section 3.2.3.

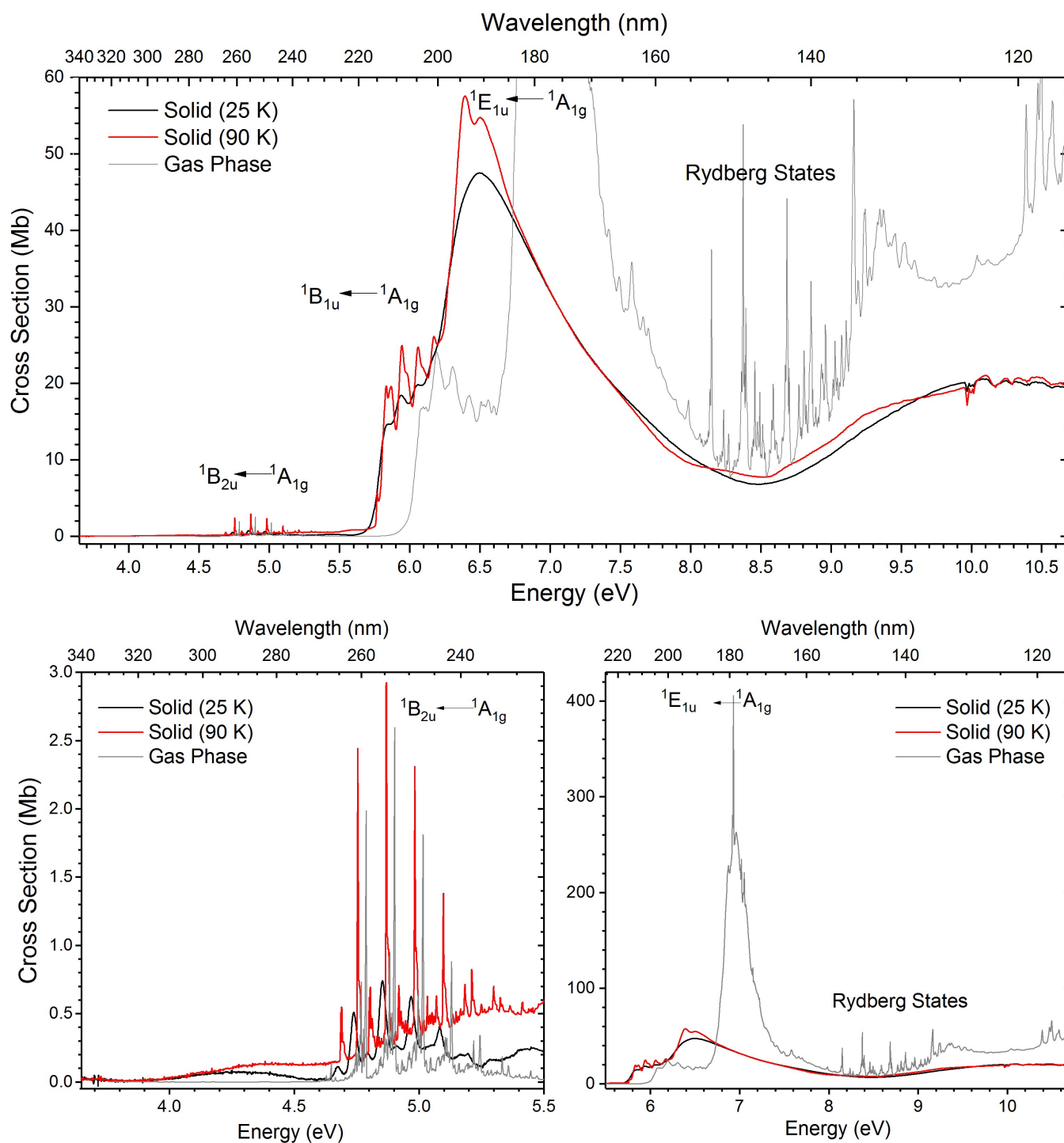


**Fig. 1 Top panel:** Overview of the vacuum ultraviolet photoabsorption spectra of benzene showing the cross sections for solid benzene deposited at 25 K (black), the same sample annealed to 90 K (red) and compared to the gas phase (grey). All three phases show three singlet-singlet electronic transitions,  ${}^1B_{2u} \leftarrow {}^1A_{1g}$ ,  ${}^1B_{1u} \leftarrow {}^1A_{1g}$  and  ${}^1E_{1u} \leftarrow {}^1A_{1g}$ , with clear redshifts observed in the solid phase spectra with respect to the gas phase. Rydberg states that can be seen in the gas phase are all suppressed in the solid phases. **Bottom left:** Zoom into the 3.6-5.5 eV region to show the vibronic bands associated with the  ${}^1B_{2u} \leftarrow {}^1A_{1g}$  transition. **Bottom right:** Zoom out of the 5.5-10.7 eV region to show the comparison between the solid phase and gas phase cross sections for the  ${}^1E_{1u} \leftarrow {}^1A_{1g}$  transition.

### 3.2 Phase change effects in solid benzene

The benzene samples deposited at 25 K were annealed to higher temperatures until changes in the spectra became visible. The spectrum of benzene was found to change between 70 and 90 K, marked by sharpening and further shifts in the bands, above which it remained unchanged until desorption. Therefore 70 K marked the onset of crystallisation from an amorphous structure initially deposited at 25 K to a crystalline structure at 90 K. Sharpening and splitting in the vibronic transitions of the  ${}^1E_{1u} \leftarrow {}^1A_{1g}$  and the  ${}^1B_{2u} \leftarrow {}^1A_{1g}$  bands are observed, with the latter being more striking. Both transitions appear to have intensities comparable to that of the gas phase and are blueshifted slightly in the  ${}^1B_{1u}$  bands and more so in the  ${}^1B_{2u}$  band relative to the amorphous 25 K spectrum, but still redshifted with respect to the gas phase.

#### 3.2.1 The ${}^1B_{2u} \leftarrow {}^1A_{1g}$ electronic transition and vibronic structure

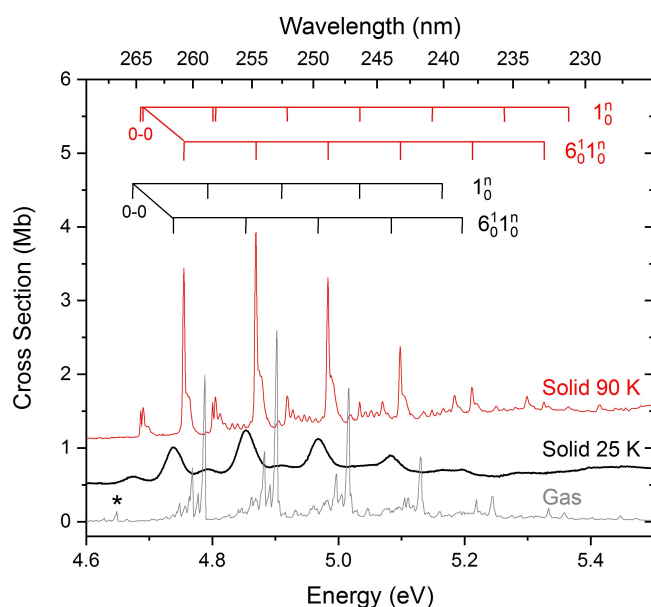


**Fig. 2** The photoabsorption spectra of the  ${}^1B_{2u} \leftarrow {}^1A_{1g}$  electronic transition of solid amorphous benzene deposited at 25 K (black) and annealed to 90 K (red) showing detailed vibronic structure and compared to the gas phase (grey). The amorphous and annealed spectra are offset vertically by 0.5 Mb for clarity. Unlike the gas phase, the electronic origin 0–0 is clearly visible in both the amorphous (25 K) and crystalline (90 K) spectra. The strongest solid phase progressions are assigned and marked with their positions and relative strengths are given in Table 1. A small peak marked with \* in the gas phase spectrum indicates the  $6_0^1$  hot band that is absent in the solid phase spectra.

The spectra of the  ${}^1B_{2u} \leftarrow {}^1A_{1g}$  electronic transition in solid and gaseous benzene are shown in Figure 2 and the main band positions and assignments of the vibronic bands are shown in Table 1. The gas phase vibronic structure is composed of a combination of fundamental vibrations, overtones, combination bands and hot bands<sup>33,34</sup>. The strongest progression observed in the gas phase spectrum is the  $6_0^1 1_0^1$  progression involving quanta of the  $\nu_1(1a_{1g})$  vibrational mode in combination with one quantum excitation of the  $\nu_6(1e_{2g})$  vibrational mode. The  $\nu_1$  vibration is the symmet-

ric breathing mode of the benzene molecule and the  $\nu_6$  vibration, known as the ‘quinoid’ mode, involves a squashing type deformation of the benzene ring and is the most efficient for inducing intensity in the bands. The next strongest transition seen in the gas phase is the progression  $6_0^1 1_0^1 1_6^1$  which involves the boat mode  $\nu_{16}(1e_{2u})$  that is an off-plane deformation.

In the spectrum of solid benzene deposited at 25 K the vibronic bands are broadened as expected due to a random distribution of bond lengths within the amorphous solid. However, surprisingly the spectrum of the annealed sample exhibits progressions of sharp vibronic bands with intensities comparable to that of the gas phase as seen in Figure 2. Despite similarities in the intensity of the  $6_0^1 1_0^1$  progression, the rest of the spectrum of the crystalline solid clearly differs from that of the gas phase. While not observed in the gas phase spectrum, the crystalline solid phase spectrum clearly shows an exciton band at the origin 0–0, which is no longer forbidden due to intermolecular interactions within the solid matrix, breaking the six-fold symmetry of the free benzene molecule, and suppression of the  $6_0^1$  hot band (see Figure 2). The position of the 0–0 band in our spectra is a well resolved sharp doublet at 4.689/4.693 eV (264.45/264.20 nm) and agrees well with the value obtained from emission and absorption spectra of crystalline benzene of 4.691 eV (264.31) by Colson *et al.*<sup>35,36</sup> and the value of 4.688/4.689 eV (264.43 nm) obtained from electron energy loss spectra of crystalline benzene at 32 K reported by Swiderek and Winterling<sup>37</sup> who also observed splitting in the band. Optical spectra of strained benzene crystals formed through careful freezing of liquid benzene to 4.2 K have also shown such splitting<sup>38,39</sup> and is attributed to Davydov crystal splitting<sup>40</sup>. Davydov provided a theoretical explanation for this by applying group theory, showing that the symmetry forbidden molecular transition to the  ${}^1B_{2u}$  state becomes allowed in the crystal and corresponds to a doublet with the electric vectors of the light aligned along two axes (*b* and *c*) of the crystal<sup>39</sup>. The unit cell of crystalline benzene contains four benzene molecules and belongs to the  $V_h^{15}$  symmetry group. The plane of the benzene ring is almost perpendicular with the *b* axis and at 40° to the *c* axis<sup>40</sup>.

The first (low energy) peak of the strongest progression in the spectrum of crystalline benzene lies 0.0684 eV from the 0–0 electronic origin equating to an infrared vibrational frequency of 551  $\text{cm}^{-1}$ . This lies near the frequency of  $\nu_6$  vibrational mode of crystalline benzene<sup>41</sup>. The average energy separation between the bands in this progression is 0.11 eV, which equals to an infrared frequency of 887  $\text{cm}^{-1}$  and lies near to the vibrational frequency of the  $\nu_1$  C–C stretch, or breathing mode of benzene, redshifted from the gas phase separation of 0.12 eV (corresponding to a vibrational frequency of around 970  $\text{cm}^{-1}$ ). This therefore suggests that the most intense progression we see in the crystalline solid phase is  $6_0^1 1_0^1$ . This is consistent with the assignment given by Colson<sup>38</sup>.

The next intense progression in the spectrum of crystalline benzene also has an average energy separation of 0.11 eV and lies 0.1147 eV from the electronic origin, consistent with the  $\nu_1$  vibration. This therefore corresponds to a totally symmetric  $\nu_1 1_0^1$  progression is built on the 0–0 transition. The other weaker pro-

**Table 1** Positions and assignments of the main vibronic bands accompanying the  ${}^1B_{2u} \leftarrow {}^1A_{1g}$  electronic transition for the sample deposited at 25 K, annealed to 90 K and compared with the gas phase and theoretical calculations together with the band areas  $\int \sigma$  relative to the  $6_0^0$  peak. The energy spacings  $\Delta E$  and energy shifts from the gas phase to the solid phase g-s are also given.

Band	Amorphous (25K)				Annealed (90K)				Gas			Calculated <sup>33</sup>		
	Position/ nm (eV)	$\Delta E$ / eV	g-s/ eV	$\int \sigma$	Position/ nm (eV)	$\Delta E$ eV	g-s/ eV	$\int \sigma$	Position/ nm (eV)	$\Delta E$ / eV	$\int \sigma$	E/ eV	$\Delta E$ / eV	$\int \sigma$
$6_0^0$	261.60 (4.74)		0.05	1.00	260.80 (4.76)		0.03	1.00	258.97 (4.79)		1.00	4.44	0.12	1.00
$6_0^1$	255.65 (4.85)	0.11	0.05	1.60	254.65 (4.87)	0.11	0.03	1.33	252.94 (4.90)	0.11	1.49	4.56	0.12	1.54
$6_0^2$	249.80 (4.96)	0.11	0.05	1.34	248.85 (4.98)	0.11	0.03	0.98	247.20 (5.02)	0.11	1.06	4.68	0.12	1.13
$6_0^3$	244.15 (5.08)	0.12	0.05	0.69	243.25 (5.10)	0.12	0.03	0.48	241.70 (5.13)	0.11	0.53	4.80	0.12	0.52
$6_0^4$	238.80 (5.19)	0.11	0.05	0.14	237.90 (5.21)	0.11	0.03	0.17	236.45 (5.24)	0.11	0.23	4.91	0.12	0.17
$6_0^5$					232.85 (5.33)	0.12	0.03	0.06	231.40 (5.36)	0.11	0.11			
0-0	265.65 (4.67)				264.45 (4.689)							4.37		
					264.20 (4.693)									
$1_0^1$	259.05 (4.79)	0.12			258.15 (4.80)	0.11								
					257.90 (4.81)									
$1_0^2$	252.75 (4.91)	0.12			251.90 (4.92)	0.11								
$1_0^3$	246.50 (5.03)	0.12			246.20 (5.04)	0.11								
$1_0^4$	240.30 (5.16)	0.13			240.75 (5.15)	0.11								
$1_0^5$					235.55 (5.26)	0.11								

gressions observed in the crystalline benzene spectrum are likely to be phonon transitions that arise due to the coupling of intramolecular vibrational modes with intermolecular lattice vibrations (phonons) with anisotropic changes in bond lengths. Contributions in intensity of the high energy wing of the bands in the progressions are thought to be due to phonon addition bands<sup>36</sup>. Assignment of the complete exciton band structure to the polarised Davydov components associated with the  ${}^1B_{2u} \leftarrow {}^1A_{1g}$  in our spectrum of crystalline benzene requires computation of density functions via the application of Frenkel exciton theory<sup>36,40</sup> and is beyond the scope of this paper.

The second weaker  $1_0^1$  progression is also visible in the amorphous solid at 25 K, albeit broadened and redshifted with respect to the crystalline spectrum. Interestingly there is also a weak broad band at 4.67 eV (265.65nm) that is consistent with the  $\nu_1$  vibrational energy spacing of the progression and the correspondingly redshifted position of the origin 0-0 compared to the 90 K crystalline benzene spectrum. The fact that the 0-0 transition is visible in the amorphous solid suggests that there exists some degree of local short-range order. The 0-0 origin was also observed around 4.69 eV (264.2 nm) in dispersed fluorescence spectra of benzene trimers formed by supersonic expansion of benzene and helium upon excitation of the  $6_0^1$  band (weaker signal) and the  $0_0^0$  band (stronger signal)<sup>42</sup>. In the same experiment the origin was not observed in the case of a monomer. Therefore intermolecular interactions in a cluster of just three benzene molecules were enough to break the symmetry to make the 0-0 origin transition allowed. Indeed since the 0-0 transition is visible in benzene trimers, intuitively we can expect to see this transition in the Van der Waals bonded amorphous solid benzene where on a macroscopic scale it is essentially composed of a random distribution of sub-ordered clusters of various sizes. Further evidence of this interesting structural effect will be discussed in Section 3.3.

### 3.2.2 The ${}^1B_{1u} \leftarrow {}^1A_{1g}$ electronic transition and vibronic structure

The spectra corresponding to the  ${}^1B_{1u} \leftarrow {}^1A_{1g}$  electronic transition of solid amorphous (25 K) and crystalline (90 K) benzene

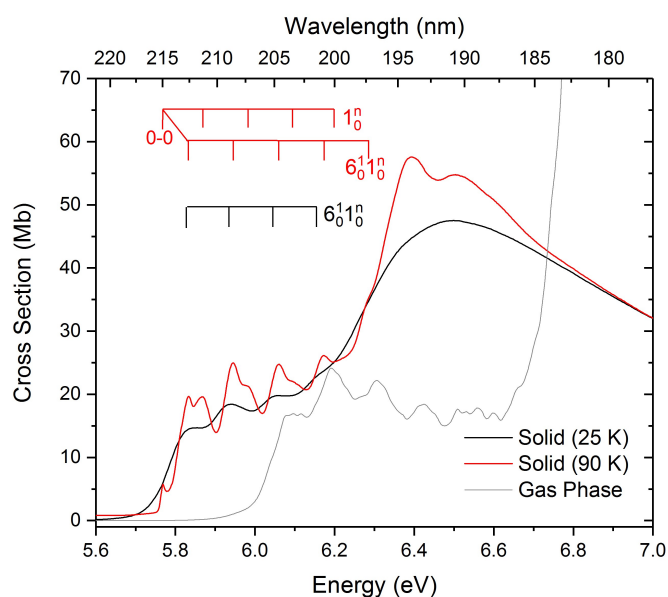


**Fig. 3** The photoabsorption spectrum of the  ${}^1B_{1u} \leftarrow {}^1A_{1g}$  electronic transition of solid amorphous benzene deposited at 25 K (black) and annealed to 90 K (red) showing detailed vibronic structure. The 0-0 band origin is clearly visible as an exciton peak in the spectrum of crystalline benzene. Band positions are marked with their positions and assignments and summarised in Table 2.

are shown in Figure 3 and compared to the gas phase spectrum. The band intensities in the solid phase are comparable to the gas phase intensities but are redshifted by 0.25 eV with respect to the gas phase (Table 2). In the gas phase this transition is also symmetry forbidden but is optically observed due to intensity borrowing from the intense  ${}^1E_{1u} \leftarrow {}^1A_{1g}$  transition. A single weak progression is visible in the spectrum of solid benzene at 25 K with a separation of 0.11 eV which equals to the infrared vibrational frequency of around  $890 \text{ cm}^{-1}$  between the vibronic bands, corresponding to the  $\nu_1$  vibrational mode. In the case of crystalline benzene at 90 K, two progressions are clearly visible. Both progressions have a separation of 0.11 eV. What is partic-

**Table 2** Positions and assignments of the main vibronic bands accompanying the  ${}^1B_{1u} \leftarrow {}^1A_{1g}$  electronic transition for the sample deposited at 25 K, annealed to 90 K and compared with the gas phase and theoretical calculations. The energy spacings  $\Delta E$  between the transition bands and energy shifts between the gas to solid phase g-s are also given.

Band	Amorphous (25K)			Annealed (90K)			Gas		Calculated <sup>33</sup>	
	Position/ nm (eV)	$\Delta E$ / eV	g-s/ eV	Position/ nm (eV)	$\Delta E$ / eV	g-s/ eV	Position/ nm (eV)	$\Delta E$ / eV	Position/ nm (eV)	$\Delta E$ / eV
$6_0^1$	212.70 (5.83)		0.24	214.09 (5.83)		0.24	204.16 (6.07)		211.84 (5.85)	0.13
$6_0^1 1_0^1$	208.80 (5.94)	0.11	0.25	210.16 (5.94)	0.11	0.25	200.30 (6.19)	0.12	207.28 (5.98)	0.13
$6_0^1 2_0^1$	204.90 (6.05)	0.11	0.26	206.19 (6.06)	0.11	0.25	196.60 (6.31)	0.12	202.90 (6.11)	0.13
$6_0^1 3_0^1$	201.20 (6.16)	0.11	0.26	202.41 (6.17)	0.11	0.25	193.00 (6.42)	0.12	198.71 (6.24)	0.13
$6_0^1 4_0^1$				198.98 (6.28)	0.11	0.26	189.80 (6.53)	0.11	194.69 (6.37)	0.13
0-0				215.05 (5.766)					216.38 (5.73)	
$1_0^1$				211.20 (5.87)	0.11					
$1_0^2$				207.20 (5.98)	0.11					
$1_0^3$				203.55 (6.09)	0.11					
$1_0^4$				199.80 (6.21)	0.11					

ularly interesting is the appearance of an exciton peak at 5.766 eV (215.05 nm). As in the case of the  ${}^1B_{2u} \leftarrow {}^1A_{1g}$  transition, this peak clearly corresponds to an electronic origin 0-0 and its position agrees well with Pantos and Hamilton<sup>43</sup> who observed the electronic origin at 5.767 eV (215.01 nm). A theoretical explanation proposed by Davydov for this<sup>40</sup> is that the forbidden transition to the level  ${}^1B_{1u}$  becomes allowed in the benzene crystal when the electric vector of light is directed along the b axis of the crystal.

There have only been a few optical studies in the literature of this  ${}^1B_{1u} \leftarrow {}^1A_{1g}$  electronic transition and vibronic progression in the solid phase and there has been some debate about the assignment of these progressions<sup>2</sup>. Theoretical calculations using first order Herzberg-Teller coupling confirm that the strongest lines in the gas phase benzene spectrum are a progression in the  $\nu_1$  vibration built upon a quantum of  $\nu_9$  ( $e_{2g}$ ) symmetric C-H bending vibration,  $9_0^1$ <sup>33,34,41</sup>. However the second peak in the progression in our spectrum of crystalline benzene lies 0.0678 eV above the 0-0 origin. This corresponds to a vibrational frequency of 547  $\text{cm}^{-1}$  which lies near the infrared position of the  $\nu_6$  ( $e_{2g}$ ) vibrational mode, the same as for the  ${}^1B_{2u}$  state in crystalline benzene discussed in section 3.2.1. Clearly the  $\nu_9$  bending mode is suppressed in the solid phase. Therefore the first progression we observe in this region of the crystalline benzene spectrum is  $6_0^1 1_0^1$ . This assignment agrees with Pantos and Hamilton<sup>43</sup>. Based on the consistent redshift in the bands between the crystalline and the amorphous solid spectra, this is also the single progression that we are observing in the amorphous benzene spectrum at 25 K. From the consistently distributed bands with equal energy separation of 0.11 eV from the 0-0 origin, the second progression in the crystalline spectrum is due to the symmetric breathing mode  $\nu_1$  with the  $1_0^1$  progression built upon the exciton peak at the origin 0-0. Unlike the  ${}^1B_{2u}$  state there is no evidence of the origin visible in the  ${}^1B_{1u} \leftarrow {}^1A_{1g}$  spectrum of amorphous benzene, however the vibronic bands are considerably broader in the region.

### 3.2.3 The ${}^3B_{1u}$ , ${}^3E_{1u}$ and ${}^3B_{2u}$ triplet states of solid benzene

Taking a closer look at the baseline in our spectra in the 3.6 to 6 eV (340 to 210 nm) region of the spectrum where the weaker spectral features lie, we see the presence of three broad diffuse bands in both the solid state spectra (Figure 4) around 4.3, 5.0 and 5.4

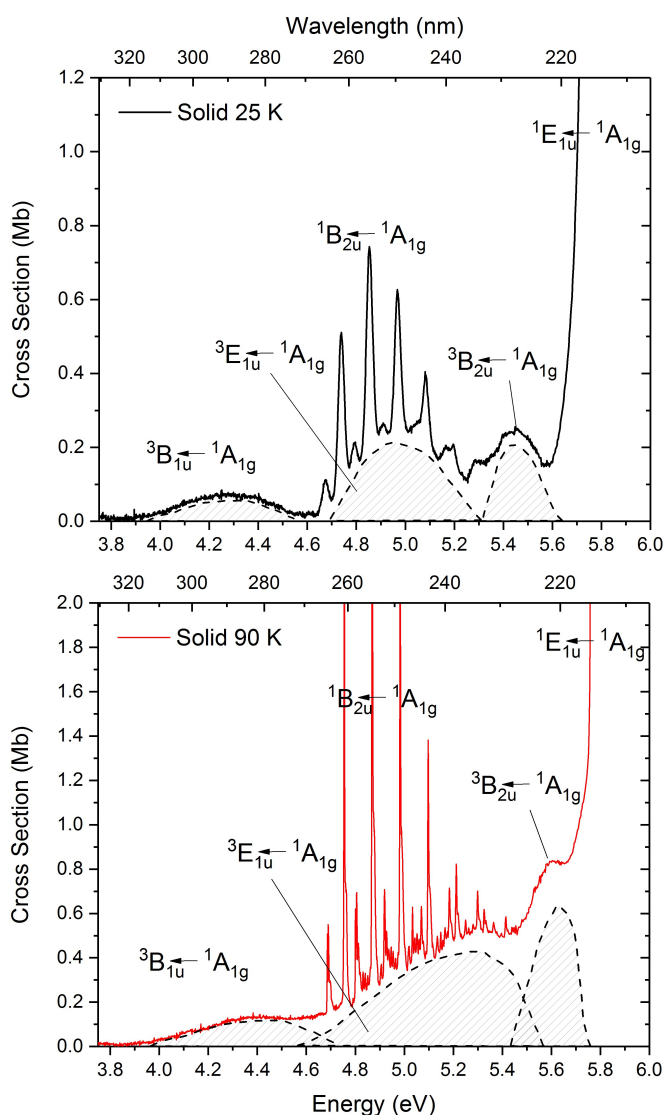


**Fig. 4** Positions of the three diffuse bands (indicated with rough sketches to guide the eye) observed in 300 nm thick solid amorphous benzene at 25 K and crystalline benzene annealed to 90 K. It is likely that these bands correspond to the lowest three spin forbidden singlet-triplet transitions to the  ${}^3B_{1u}$ ,  ${}^3E_{1u}$  and  ${}^3B_{2u}$  states.

**Table 3** Positions of the bands corresponding to three singlet-triplet states  $^3B_{1u}$ ,  $^3E_{1u}$  and  $^3B_{2u}$  from literature compared to the positions of the diffuse bands we observe in our spectra. Values marked with \* are averaged band positions or positions of the central vibrational band. Values marked with † are averaged values across different studies (all in agreement to within a few meV).

Sample	Band positions in nm (eV)		
	$^3B_{1u}$	$^3E_{1u}$	$^3B_{2u}$
Photoabsorption spectroscopy:			
Amorphous solid (25 K)	4.3	5.0	5.4
Crystalline solid (90 K)	4.4	5.3	5.6
Thick crystal (4.2 K) <sup>32</sup>	3.7*	4.6*	
O <sub>2</sub> perturbed crystal <sup>32</sup>	3.8*	4.5*	
O <sub>2</sub> perturbed (gas) <sup>50</sup>	3.9		
NO perturbed crystal <sup>51</sup>		4.6*	
Electron impact:			
Gas <sup>47–49</sup>	3.9†	4.8†	5.7†
Amorphous solid (32 K) <sup>37</sup>	3.66		
	3.77		
	3.89		
	3.99		
	3.85 avg.		
Crystalline solid (100 K) <sup>37</sup>	3.68		
	3.79		
	3.90		
	4.01		
	3.83 avg.		

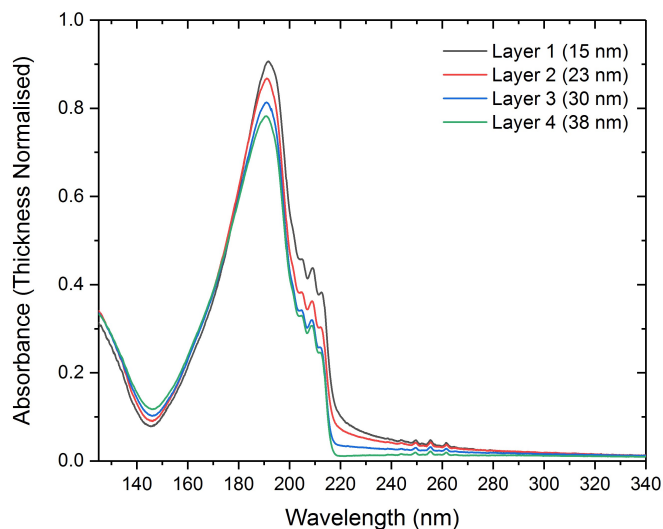
eV (290, 250 and 228 nm) in the amorphous solid at 25 K and 4.4, 5.3 and 5.6 eV (282, 234 and 221 nm) in the annealed crystalline solid at 90 K. These bands are more obvious in the thicker samples and it is clear that, consistent with singlet-singlet transitions, they are blueshifted from the amorphous to crystalline phase and accompanied with an increase in intensity. We believe that these bands could be the theoretically predicted three lowest lying spin-forbidden singlet-triplet transitions of benzene corresponding to transitions from the singlet ground state to the  $^3B_{1u}$ ,  $^3E_{1u}$  and  $^3B_{2u}$  states. Optically it is difficult to observe these transitions in the gas phase and at high temperatures as they lie close to hot bands associated with the intense singlet-singlet transitions. Since hot bands are suppressed in low temperature matrices, this could explain why these singlet-triplet transitions are visible in our spectra. Spin forbidden triplet states, arising from spin-orbit coupling<sup>44,45</sup>, have been investigated using a variety of techniques in the gas phase including low energy, high scattering angle electron impact<sup>46–49</sup>, photoabsorption spectroscopy via high pressure (100 atm) doping of benzene vapour with oxygen<sup>50</sup> and photoabsorption spectroscopy of thick pure benzene crystals cooled from the liquid phase to 4.2 K<sup>32</sup> and the same doped with small amounts (2%) of oxygen<sup>32</sup> or nitric oxide<sup>51</sup>. Singlet-triplet transitions have not yet, to our knowledge, been reported in photoabsorption spectra of amorphous benzene. We found only one study in the literature reported by Swiderek and Winterling<sup>37</sup> that describes the lowest singlet-triplet transition in amorphous and crystalline benzene films deposited on polycrystalline on a platinum substrate using electron-energy-loss spectroscopy.

Table 3 summarises the positions of the triplet bands reported in the literature with comparison to the position of the bands that we see in our spectra. All gas-phase studies show vibrational

bands associated with the singlet-triplet transitions. These are not reported for the solid phases of benzene except in the electron impact study of Swiderek and Winterling<sup>37</sup>. The positions of the triplet states agree to within a few meV in all of the gas phase electron scattering experiments. It can be seen from table 3 that the positions of our bands in amorphous benzene are all blueshifted by between 0.2 and 0.3 eV with respect to the gas phase positions measured by electron impact. There are few studies in the solid phase and more discrepancy is seen between the different techniques used. Though the positions of our bands do not agree with the solid phase data in the literature, Swiderek and Winterling also report a blueshift in going from the amorphous to the crystalline phase, as we observe in our spectra, though the shift they observe is small (0.02 eV) compared to a shift of between 0.1 and 0.3 eV that we observe. The differences in the results may be attributed to differences in sample preparation. Our crystalline samples were formed by annealing benzene from 25 K to 90 K whereas Swiderek and Winterling deposited their samples at 100 K. We know from a previous photoabsorption study of ammonia ice<sup>28</sup>, for instance, that strikingly different photoabsorption spectra are observed when ammonia is deposited above crystallisation temperature to that of ammonia annealed from an amorphous phase to temperatures above crystallisation and such differences reflect the different morphologies of the crystalline solid formed. Furthermore, the samples grown by Swiderek and Winterling were thin (less than 27 monolayers) as per experimental requirement compared to the thick (300 nm) samples required to see these bands in our spectra, and as will be shown in the next section, amorphous benzene exhibits structural effects as a function of sample thickness. The blueshift that we observe in the bands between the amorphous and crystalline spectra strongly suggest an effect that is linked to the phase change in the solid, such as the redshifts that are seen in the singlet-singlet transition bands. Taking into account the evidence above and given the lack of consistent solid phase data in the literature, we can tentatively say that the bands we observe in our spectra are good candidates for assignment to the  $^1B_{1u} \leftarrow ^1A_{1g}$ ,  $^3E_{1u} \leftarrow ^1A_{1g}$  and  $^3B_{2u} \leftarrow ^1A_{1g}$  singlet-triplet transitions. Further detailed investigation is required to understand the origin of these singlet-triplet transitions.

### 3.3 Thickness effects

We investigated the effect of sample thickness on the photoabsorption spectra of thin (tens of nm) films of benzene. Samples were deposited layer by layer and the spectra were measured after each successive deposition. The spectra of solid benzene at four different thicknesses are shown in Figure 5. It can clearly be seen that there is a thickness dependent tail on the red wing of the band due to the strong  $^1E_{1u} \leftarrow ^1A_{1g}$  electronic transition. The strength of the scattering effect decreases with each successive deposition and vanishes after the fourth deposition. Scattering in ultraviolet spectra are predominantly Rayleigh scattering due to particles that are less than  $\lambda/10$  in size and has a  $1/\lambda^4$  relationship as a function of wavelength. This would suggest that benzene is not growing in a uniform layer, but is forming ‘clumps’



**Fig. 5** Photoabsorption spectra of successive benzene layers deposited at 25 K on a magnesium fluoride window. The spectra are normalised to sample thickness to check for any variation as a function of sample thickness. A thickness dependent scattering tail is clearly visible  $>210$  nm on the red wing of the strong  ${}^1B_{1u} \leftarrow {}^1A_{1g}$  absorption band.

**Table 4** Results of the Rayleigh scattering fit from the model shown in equation 5. \*The error in the constant  $c$  for layer 4 was too high due to a poor fit as scattering is diminished in this layer.  $b$  in equation 5 is a baseline correction parameter which was negligible and ranged between  $(4.1 \pm 0.1) \times 10^{-6}$  and  $(1.01 \pm 0.05) \times 10^{-5}$ . Values of  $a^6$ , proportional to the size of scatterers are given in the last column

Layer	Thickness (nm)	$c$ ( $\times 10^{-2}$ )	$a$ ( $\times 10^8$ )	$a^6$ ( $\text{nm}^2$ )
1	15	$0.026 \pm 0.0001$	$21.40 \pm 0.001$	35.9
2	23	$0.041 \pm 0.001$	$18.37 \pm 0.010$	34.9
3	30	$0.750 \pm 0.391$	$1.08 \pm 0.550$	21.8
4	38	1*	$0.78 \pm 0.001$	20.7
new	16	$0.0355 \pm 0.0002$	$21.03 \pm 0.003$	35.8

on the surface. It is clear from the presence of scattering in our spectra that benzene therefore does not wet the substrate.

In order to verify the nature of scattering we have fitted a simple Rayleigh model to the tails of our electronic spectra for  $\lambda > 220$  nm by considering the transmitted intensity  $I_t$  as being the incident intensity  $I_0$  minus the scattered intensity  $I_{scat}$ , where  $I_{scat} \propto \lambda^{-4}$ . So by rewriting Equation 2 as

$$A = \ln \left( \frac{I_0(\lambda)}{I_0(\lambda) - a\lambda^{-4}} \right) \quad (4)$$

We can fit a function of the form

$$A = c \ln \left( \frac{1}{1 - a\lambda^{-4}} \right) + b \quad (5)$$

to the scattering tails of our spectra in the region 220–340 nm, avoiding the onset of the strong absorption band near 220 nm. Here the constant  $a$  is proportional to  $r^6$ , where  $r$  is the scattering particle size and  $c$  is proportional to the number density of the scatterers in the beam path.

The fits to the spectra and the residuals are shown in Figure 6 and the results of the fits are summarised in Table 4. The

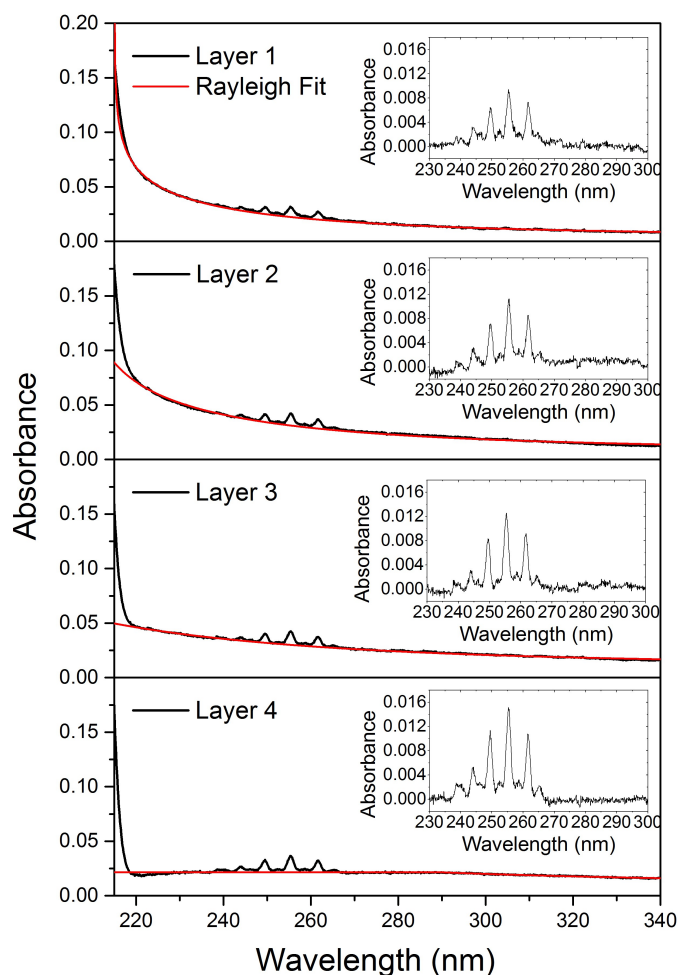


**Fig. 6** Rayleigh scattering fits to the tails ( $>220$  nm) of the un-normalised spectra shown in Figure 5 with residuals shown in the inset. The fit parameters are summarised in Table 4.

fits indeed confirm that the scattering must be due to benzene ‘nanoparticles’ and from the combination of the fits and the thickness of benzene deposited derived from laser interference measurements, we estimate the sizes of the benzene ‘clumps’ in the thinnest layers to be less than 10 nm.

From the results in Table 4 we can see that parameter  $a$ , which relates to the sizes of the particles remains roughly the same as film thickness increased from 15 nm in layer 1 to 23 nm in layer 2, however the parameter  $c$  almost doubles, suggesting that the number of ‘clumps’ has increased while the size of the ‘clumps’ remained roughly the same. As the thickness was increased from 23 nm to 30 nm parameter  $a$  decreased by an order of magnitude, corresponding to a decrease in particle size by a factor of 1.6. At the same time the number density of the scattering particles increased significantly until by layer 4 (38 nm) the sample reached the regime of a bulk solid film, however still registering some clumping with scatterers of a finite size present within the ice suggesting a granular morphology.

During another beamtime run at ASTRID2 a year later we prepared a sample with a thickness of 16 nm to check for consistency. If we compare parameters  $a$  and  $c$  with of this ‘new’ sample

with that of layers 1 and 2, we can clearly see that the values of the parameters fit the trend. This supports the model of finite sized grains formed due to non-wetting of the substrate, with the number of grains increasing with increasing sample thickness and grain size decreasing as we begin to reach a bulk solid regime.

Evidence of 'non-wetting' or 'islanding' of benzene adsorbed to different substrates has been reported in other studies, albeit at higher temperatures. Thrower *et. al.*<sup>52</sup> reported this effect in their study of photon stimulated desorption of vapour deposited benzene and water layers on sapphire at 80 K, suggesting that benzene was not wetting the sapphire substrate and also formed islands when benzene was deposited on top of water. Thrower<sup>53</sup> have also observed 'islanding' effects in a temperature programmed desorption study of benzene deposited on silicate grain surfaces at 115 K. Such 'islanding' effects suggest that benzene molecules are fairly mobile and are able to diffuse along the surface. Stranick *et. al.*<sup>54</sup> reported evidence of 2D gas behaviour of benzene by observing the dynamics of benzene molecules adsorbed on copper (Cu111) at 77 K using scanning tunnelling microscopy (STM). In a study of benzene diffusion of sub-monolayer films of benzene deposited on graphite surfaces at 140 K, Fouquet *et. al.*<sup>55</sup> suggest that an observed coverage dependent change in the speed of diffusion of benzene molecules on the surface can be attributed to weak substrate-molecule interactions thereby enhancing molecule-molecule attraction. Such effects observed in the sub-monolayer regime can intuitively suggest that higher coverages will cause 'islanding' and 'cluster' growth. Evidence of '3D clusters' was reported by Bahr *et. al.*<sup>56</sup> in a temperature programmed desorption and metastable impact electron spectroscopy study of the interaction of benzene with amorphous solid water adsorbed on polycrystalline silver substrate at 124 K. Interestingly the authors report that although the first layer of benzene aligns parallel to the silver surface, during the formation of the second layer the benzene molecular planes are tilted with respect to the first layer. This points to possible surface reconstruction effects and the onset of '3D cluster' formation.

All of the above experiments were carried out at higher temperatures (77-140 K) and show evidence of 'island' formation and '3D cluster growth'. At low temperatures the diffusion of molecules at the surface is negligible *et. al.*<sup>55</sup>. Therefore, without further study it is not possible to ascertain the exact mechanism that gives rise to the formation of clumps in our samples of benzene deposited at 20 K. However, evidence from our results strongly suggests the formation of benzene clumps or clusters, giving rise to reproducible strong Rayleigh scattering tails as a function of coverage. This suggests that there is a 3D growth effect resulting in surface roughness composed of benzene nano-clusters. The parameters derived from the scattering fits suggest that the clusters must reach a maximum finite size as further deposition does not appear to result in the growth of the size of the clumps (as the size parameter below a thickness of 30 nm remains roughly the same), instead there is an increase in the number of clumps as evidenced by an increase in the number density of the scatterers. The film reaches what appears to be a 'bulk' ice regime via increasing number of clumps and decreasing clump size, possibly due to successive benzene adsorption 'filling in' the gaps between the

underlying 3D clumps. Furthermore, we observe weak exciton-exciton transitions in the amorphous ice at 25 K in the associated with the  ${}^1B_{1u} \leftarrow {}^1A_{1g}$  transition, suggesting that some degree of local order must exist on a microscopic scale, possibly within finite '3D clusters', within the macroscopic amorphous matrix. This may subsequently lead efficient surface reconstruction at higher temperatures, via the rearrangement of benzene molecules, giving rise to the observed very sharp and well defined exciton peaks and crystal field Davydov splitting in the annealed benzene sample. In our previous study of ammonia ice films<sup>28</sup> we observed an exciton peak only when ammonia was deposited at the crystallisation temperature (75 K). The exciton peak was not reproducible in samples that were deposited at 25 K and subsequently annealed to 75 K. This suggests that unlike ammonia, the weaker intermolecular interactions between benzene molecules allow for efficient rearrangement of the solid matrix. Further studies (that are beyond the scope of this paper) employing the use of other surface experimental techniques such as RAIRS and TPD, imaging techniques such as atomic force microscopy (AFM) and scanning electron microscopy (SEM) as well as a theoretical approach are required to fully understand the thickness dependent 3D growth mechanism of benzene at low temperatures that gives rise the scattering observed.

It is clear from the photoabsorption spectra of benzene and evidence from the scattering data, that there is strong coupling between the intermolecular lattice vibrations and intramolecular vibronic states, linked to the macroscopic structure of condensed benzene and hence the structure of benzene will greatly influence photochemical processes.

## 4 Summary and Conclusions

We have carried out a detailed study of the photoabsorption spectrum of solid benzene vapour deposited at 25 K and annealed to crystallisation temperature (90 K). This study forms a part of a wider experimental programme aimed at understanding the influence of polycyclic aromatic hydrocarbons (PAHs) on photochemistry in such environments, as well as their role in defining the physical and chemical properties of ices. Benzene is the first species selected in this study as a prototypical aromatic molecule and we probe the electronic structure of this molecular ice in both the amorphous and crystalline form. Our results show that there is a significant change in the solid phase spectra of benzene compared to the gas phase with further variations observed between the amorphous and crystalline phases. The summary of our results are:

- The bands corresponding to singlet-singlet transitions in solid amorphous benzene from the  ${}^1A_{1g}$  ground state to the electronically excited  ${}^1E_{1u}$ ,  ${}^1B_{1u}$  and  ${}^1B_{2u}$  states are all red-shifted with respect to the gas phase spectrum by 0.51, 0.25 and 0.05 eV respectively.
- While the positions of the  ${}^1E_{1u} \leftarrow {}^1A_{1g}$  and  ${}^1B_{1u} \leftarrow {}^1A_{1g}$  bands remain the same for both amorphous and crystalline benzene, a further redshift of 0.02 eV in the bands associated with the  ${}^1B_{2u} \leftarrow {}^1A_{1g}$  is observed in amorphous benzene.

- We have observed vibrational structure associated with the lowest lying symmetry forbidden  ${}^1B_{2u} \leftarrow {}^1A_{1g}$  electronic transition in both crystalline and amorphous benzene, consisting of the first intense  $6_0^1 1_0^n$  vibronic progression and the second intense  $1_0^n$  transition built upon the 0–0 electronic origin exciton transition. The 0–0 electronic origin has not previously been reported in amorphous benzene.
- The  ${}^1B_{2u} \leftarrow {}^1A_{1g}$  structure in crystalline benzene also exhibits Davydov crystal splitting and phonon contributions due to intermolecular interactions.
- We have observed vibrational structure associated with the second symmetry forbidden  ${}^1B_{1u} \leftarrow {}^1A_{1g}$  electronic transition. A weak broad  $6_0^1 1_0^n$  transition is observed in amorphous benzene, whereas two distinct sharper progressions  $6_0^1 1_0^n$  and  $1_0^n$  are seen in the spectrum of crystalline benzene built upon a sharp 0–0 electronic origin exciton peak.
- We observed three diffuse bands in thick (300 nm) amorphous and crystalline benzene spectra that we tentatively assign to the spin-forbidden singlet–triplet transitions from the  ${}^1A_{1g}$  ground state to the  ${}^3B_{1u}$ ,  ${}^3E_{1u}$  and  ${}^3B_{2u}$  states. The bands are blueshifted with respect to the gas phase positions determined by electron scattering experiments and a further blueshift is observed in going from an amorphous to a crystalline solid.
- Thinner amorphous benzene samples (less than 40 nm) exhibit thickness dependent Rayleigh scattering tails for wavelengths greater than 200 nm showing evidence of non-uniform film growth and island formation. Fits to the scattering tails also reveal reconstruction effects within the solid with increasing thickness.

Exploiting the knowledge and the tools of physical chemistry to study low temperature molecular ice films is important in understanding the physico-chemical properties of ices in astrochemical and planetary environments. It also allows us to evaluate the techniques that are typically used to create such ice analogues and questions whether such techniques produce adequately realistic mimics. Vacuum ultraviolet spectroscopy provides invaluable information not only about the intramolecular electronic structure of these ices but also of their intermolecular interactions and macroscopic structure. In this paper we investigated the properties of solid benzene as part of an ongoing programme to investigate the physico-chemical properties of various ices. Often the physical chemistry/chemical physics journals are not easily accessible to astronomers and we aim to draw out the important information from our work to inform astronomers and modelers in the astrochemistry and planetary science community.

It important to stress here that experimental high resolution photoabsorption spectroscopy is vital for the study of photochemical processes under astrophysical conditions, such as for example the phenomenon of benzene-facilitated desorption<sup>52</sup>. This experiment relied on high resolution VUV spectra of solid benzene that were measured by our group at the time but not published (referred as a private communication by<sup>52</sup>). The excitation energy

selected for resonant excitation of the  $6_0^1 1_0^2$  vibronic state at 248.8 nm is clearly highly dependent on the sample temperature, and could not be derived from the gas phase. Resonant excitation of this band with a laser, in the spectral region where water absorption is negligible, resulted in the desorption of benzene with a translational energy of 1200 K, but also in the desorption of ‘hot’ water molecules, with a translational energy of 450 K, after transfer of energy from benzene to water.

We can see from the results presented here that there are significant gas–solid shifts in the bands corresponding to the electronic transitions of benzene and that the band positions and in some cases the cross sections depend on the morphology of benzene ice. The integrated cross section of the most intense  $\pi^* \leftarrow \pi$  electronic transition  ${}^1E_{1u} \leftarrow {}^1A_{1g}$  is 50% lower in the solid than that of the gas phase and redshifted by 0.51 eV. This will affect results of photodesorption rates and kinematic studies involving UV photoprocessing of ice films involving benzene. With their very high UV cross-sections, benzene and PAH’s are likely to be very influential in photochemical and photodesorption processes within ice mantles via electronic and vibronic excitation and dissipation of energy to the surrounding matrix. It is clear from our data that there is considerable coupling between the intramolecular vibrational modes and the intermolecular lattice vibrations in both crystalline and amorphous benzene.

Benzene is the building block of polycyclic aromatic hydrocarbons (PAH’s) that are abundant in the interstellar medium. It is possible therefore that at low temperatures (10–20 K) that these molecules will clump together forming nano-particles, contributing to UV scattering and extinction, and providing nucleation sites for atomic and simple molecular adsorbates such as water and carbon monoxide. We have seen from our results that there are interesting thickness-dependent scattering effects in thin layers of benzene (less than 40 nm) with evidence of clumping, resulting in a granular morphology. Furthermore, this effect would significantly influence the results of traditional laboratory astrochemistry experiments, where vapour deposited films are investigated, as the structure and morphology of the film is likely to impact on the physical and chemical processes under investigation.

Finally, with spin forbidden optical transitions becoming allowed in the solid phase, new chemical channels will become available that are otherwise forbidden in the gas phase. Of course ices in the ISM are not pure ices and are mixtures dominated by water - the most abundant constituent of astrochemical ices. Therefore we are exploring benzene–water layers and mixtures with results to be presented in a subsequent publication.

## 5 Acknowledgements

The authors acknowledge the CALIPSO programme for contributing towards access to ASTRID2 Facility, Denmark. AD acknowledges Science and Technology Facilities Council and the Open University for co-funding her Daphne Jackson Fellowship. We thank NCJ for measuring and providing the gas phase benzene spectrum used for comparison in this study.

## References

- 1 T. Dunn, *Studies on Chemical Structure and Reactivity*, New York, Wiley, 1966, p. 103.
- 2 M. B. Robin, *Higher Excited States of Polyatomic Molecules*, Academic Press, 1975, pp. 209–268.
- 3 W. A. Brown, *Physical Chemistry Chemical Physics*, 2014, **16**, 3343–3343.
- 4 N. J. Mason, A. Dawes, P. D. Holtom, R. J. Mukerji, M. P. Davis, B. Sivaraman, R. I. Kaiser, S. V. Hoffmann and D. A. Shaw, *Faraday discussions*, 2006, **133**, 311–329.
- 5 A. G. Tielens, *Annu. Rev. Astron. Astrophys.*, 2008, **46**, 289–337.
- 6 A. Tielens, *Reviews of Modern Physics*, 2013, **85**, 1021.
- 7 J. Cernicharo, A. M. Heras, A. Tielens, J. R. Pardo, F. Herpin, M. Guélin and L. Waters, *The Astrophysical Journal Letters*, 2001, **546**, L123.
- 8 J. Bernard-Salas, E. Peeters, G. Sloan, J. Cami, S. Guiles and J. Houck, *The Astrophysical Journal Letters*, 2006, **652**, L29.
- 9 V. Geers, E. Van Dishoeck, K. Pontoppidan, F. Lahuis, A. Crapsi, C. Dullemond and G. Blake, *Astronomy & Astrophysics*, 2009, **495**, 837–846.
- 10 S. Sandford, M. Bernstein and L. Allamandola, *The Astrophysical Journal*, 2004, **607**, 346.
- 11 S. A. Sandford, *Planetary and Space Science*, 2002, **50**, 1145–1154.
- 12 B. Acke and M. E. van den Ancker, *Astronomy & Astrophysics*, 2004, **426**, 151–170.
- 13 V. Geers, J.-C. Augereau, K. Pontoppidan, C. Dullemond, R. Visser, J. Kessler-Silacci, N. Evans II, E. van Dishoeck, G. Blake, A. Boogert *et al.*, *Astronomy & Astrophysics*, 2006, **459**, 545–556.
- 14 I. Kamp and I. Kamp, *EAS Publications Series*, 2011, **46**, 271–283.
- 15 D. P. Cruikshank, C. M. Dalle Ore, R. N. Clark and Y. J. Pendleton, *Icarus*, 2014, **233**, 306–315.
- 16 A. Li, *Deep Impact as a World Observatory Event: Synergies in Space, Time, and Wavelength*, Springer, 2009, pp. 161–175.
- 17 J. H. Hahn, R. Zenobi, J. L. Bada and R. N. Zare, *Science*, 1988, **239**, 1523–1525.
- 18 S. J. Clemett, C. R. Maechling, R. N. Zare, P. D. Swan and R. M. Walker, *Science*, 1993, **262**, 721–725.
- 19 C. Sagan, B. Khare, W. Thompson, G. McDonald, M. R. Wing, J. L. Bada, T. Vo-Dinh and E. Arakawa, *The Astrophysical Journal*, 1993, **414**, 399–405.
- 20 M. S. Gudipati and L. J. Allamandola, *The Astrophysical Journal Letters*, 2003, **596**, L195.
- 21 M. S. Gudipati and L. J. Allamandola, *The Astrophysical Journal Letters*, 2004, **615**, L177.
- 22 J. Bouwman, H. M. Cuppen, A. Bakker, L. J. Allamandola and H. Linnartz, *Astronomy & Astrophysics*, 2010, **511**, A33.
- 23 M. S. Gudipati and L. J. Allamandola, *The Astrophysical Journal*, 2006, **638**, 286.
- 24 M. P. Bernstein, M. H. Moore, J. E. Elsila, S. A. Sandford, L. J. Allamandola and R. N. Zare, *The Astrophysical Journal Letters*, 2003, **582**, L25.
- 25 J. Bouwman, D. Paardekooper, H. Cuppen, H. Linnartz and L. Allamandola, *The Astrophysical Journal*, 2009, **700**, 56.
- 26 J. Thrower, B. Jørgensen, E. E. Friis, S. Baouche, V. Mennella, A. Luntz, M. Andersen, B. Hammer and L. Hornekær, *The Astrophysical Journal*, 2012, **752**, 3.
- 27 P. Holtom, A. Dawes, R. Mukerji, M. Davis, S. Webb, S. Hoffman and N. Mason, *Physical Chemistry Chemical Physics*, 2006, **8**, 714–718.
- 28 A. Dawes, R. J. Mukerji, M. P. Davis, P. D. Holtom, S. M. Webb, B. Sivaraman, S. V. Hoffmann, D. A. Shaw and N. J. Mason, *The Journal of chemical physics*, 2007, **126**, 244711.
- 29 M. H. Palmer, T. Ridley, S. V. Hoffmann, N. C. Jones, M. Coreno, M. De Simone, C. Grazioli, M. Biczysko, A. Baiardi and P. Limão-Vieira, *The Journal of chemical physics*, 2015, **142**, 134302.
- 30 M. Westley, G. Baratta and R. Baragiola, *The Journal of chemical physics*, 1998, **108**, 3321–3326.
- 31 K. Moutzouris, M. Papamichael, S. C. Betsis, I. Stavrakas, G. Hloupis and D. Triantis, *Applied Physics B*, 2014, **116**, 617–622.
- 32 S. D. Colson and E. R. Bernstein, *The Journal of Chemical Physics*, 1965, **43**, 2661–2669.
- 33 A. Bernhardsson, N. Forsberg, P.-Å. Malmqvist, B. O. Roos and L. Serrano-Andrés, *The Journal of Chemical Physics*, 2000, **112**, 2798–2809.
- 34 T. J. Penfold and G. A. Worth, *The Journal of chemical physics*, 2009, **131**, 064303.
- 35 E. R. Bernstein, S. Colson, R. Kopelman and G. Robinson, *The Journal of Chemical Physics*, 1968, **48**, 5596–5610.
- 36 S. Colson, D. Hanson, R. Kopelman and G. Robinson, *The Journal of Chemical Physics*, 1968, **48**, 2215–2231.
- 37 P. Swiderek and H. Winterling, *Chemical physics*, 1998, **229**, 295–307.
- 38 S. D. Colson, *The Journal of Chemical Physics*, 1966, **45**, 4746–4747.
- 39 S. D. Colson, *The Journal of Chemical Physics*, 1968, **48**, 3324–3332.
- 40 A. Davydov, *Theory of molecular excitons*, Springer, 1962.
- 41 G. Kearley, M. Johnson and J. Tomkinson, *The Journal of chemical physics*, 2006, **124**, 044514.
- 42 P. R. Langridge-Smith, D. V. Brumbaugh, C. A. Haynam and D. H. Levy, *The Journal of Physical Chemistry*, 1981, **85**, 3742–3746.
- 43 E. Pantos and T. Hamilton, *Chemical Physics Letters*, 1972, **17**, 588–591.
- 44 B. R. Henry and W. Siebrand, *The Journal of Chemical Physics*, 1971, **54**, 1072–1085.
- 45 G. W. Robinson, *The Journal of Chemical Physics*, 1967, **46**, 572–585.
- 46 J. P. Doering, *The Journal of Chemical Physics*, 1969, **51**, 2866–2870.
- 47 J. Doering, *The Journal of Chemical Physics*, 1977, **67**, 4065–

- 4070.
- 48 D. G. Wilden and J. Comer, *Journal of Physics B: Atomic and Molecular Physics*, 1980, **13**, 627.
- 49 H. Kato, M. Hoshino, H. Tanaka, P. Limão-Vieira, O. Ingólfsson, L. Campbell and M. J. Brunger, *The Journal of chemical physics*, 2011, **134**, 134308.
- 50 D. Evans, *Journal of the Chemical Society (Resumed)*, 1957, 1351–1357.
- 51 E. R. Bernstein and S. D. Colson, *The Journal of Chemical Physics*, 1966, **45**, 3873–3873.
- 52 J. Thrower, D. Burke, M. Collings, A. Dawes, P. Holtom, F. Jamme, P. Kendall, W. Brown, I. Clark, H. Fraser *et al.*, *The Astrophysical Journal*, 2008, **673**, 1233.
- 53 J. Thrower, M. Collings, F. Rutten and M. McCoustra, *Monthly Notices of the Royal Astronomical Society*, 2009, **394**, 1510–1518.
- 54 S. J. Stranick, M. M. Kamna and P. S. Weiss, *Science*, 1994, **266**, 99–102.
- 55 P. Fouquet, M. R. Johnson, H. Hedgeland, A. P. Jardine, J. Ellis and W. Allison, *Carbon*, 2009, **47**, 2627–2639.
- 56 S. Bahr and V. Kempter, *The Journal of chemical physics*, 2007, **127**, 074707.